ADVANCED ENERGY MATERIALS
www.advenergymat.de

Rationalizing Electron–Phonon Interactions and Hot Carriers Cooling in 2D to 3D Metal Halide Perovskites

Arup Mahata, Edoardo Mosconi, Daniele Meggiolaro,* Simona Fantacci, and Filippo De Angelis**

The cooling mechanism of hot carriers (HC) in metal halide perovskites is a topic of debate which gathered huge attention due to its critical role in the performance of perovskite-based optoelectronics. HC cooling in 2D perovskites is faster than in its 3D counterpart, whereas in 2D/3D perovskites cooling becomes faster with decreasing the thickness of the inorganic quantum wells. Using state-of-the art first principles calculations it is showed that the modulation of electron–phonon (e-ph) coupling strength between bending and stretching phonon branches can explain this observation. Starting from the prototype BA_2PbI_4 and PEA_2PbI_4 2D perovskites, e-ph coupling of individual phonon modes is investigated for 2D/3D perovskites with $n = 1$ and 3, along with a vis-à-vis comparison with the prototypical 3D $MAPbI_3$ system. This study shows that e-ph coupling with high-frequency stretching phonon modes in the 60–120 cm^{-1} range is highest for $n = 1$ while it decreases with increasing the quantum well layers, by approaching the 3D bulk limit where e-ph coupling with low-frequency bending phonon modes (<60 cm^{-1}) is dominant. Longer spacer cations with identical quantum well structures have a limited impact on the e-ph coupling, highlighting that the primary factor governing HC cooling is the quantum confinement within the inorganic sublattice. This study provides an advancement in the understanding of the mode-specific e-ph mediated HC cooling mechanism in metal-halide perovskites and can provide a route map toward tuning the e-ph interaction, which is instrumental for effectively gathering HC in solar cell devices.

1. Introduction

Metal-halide perovskites have emerged as a promising class of semiconducting materials for optoelectronic applications.[1,2] Charge-carrier dynamics in such materials is controlled by the cooling rate of hot carriers (HC). In solar cells, photons possessing energies larger than the absorber's bandgap can form free carriers with initial excess kinetic energies at least k_BT above the band edges.[3] HC are at a non-equilibrium state, undergoing a rapid ≈picoseconds cooling to the band edges by losing their excess kinetic energies before becoming available for charge extraction.[4,5] HC cooling is one of the major reasons for efficiency loss in solar cells.[3,6] Such loss can be avoided if the HC can be utilized before they equilibrate and, in this way the thermodynamic Shockley-Queisser limit of 33% on conversion efficiency can be ideally improved up to ≈66%.[3,7]

Using transient absorption (TA) spectroscopy, Xing et al. first reported a 0.4 ps HC cooling time in $MAPbI_3$.[8] Later on, depending on photoexcited carrier density, a surprisingly long-lived

A. Mahata, E. Mosconi, D. Meggiolaro, S. Fantacci, F. De Angelis
Computational Laboratory for Hybrid/Organic Photovoltaics (CLHYO)
Istituto CNR di Scienze e Tecnologie Chimiche (SCITEC-CNR)
Via Elce di Sotto 8, Perugia 06123, Italy
E-mail: arup@chy.iith.ac.in; daniele.meggiolaro@cnr.it; filippo@thch.unipg.it

A. Mahata
Department of Chemistry
Indian Institute of Technology Hyderabad
Kandi, Sangareddy, Telangana 502285, India

F. De Angelis
Department of Chemistry, Biology and Biotechnology
University of Perugia
Via Elce di Sotto 8, Perugia 06123, Italy

F. De Angelis
Department of Mechanical Engineering
College of Engineering
Prince Mohammad Bin Fahd University
P.O. Box 1664, Al Khobar 31952, Kingdom of Saudi Arabia

F. De Angelis
SKKU Institute of Energy Science and Technology (SIEST)
Sungkyunkwan University
Suwon 440-746, South Korea

The ORCID identification number(s) for the author(s) of this article can be found under https://doi.org/10.1002/aenm.202303405

DOI: 10.1002/aenm.202303405

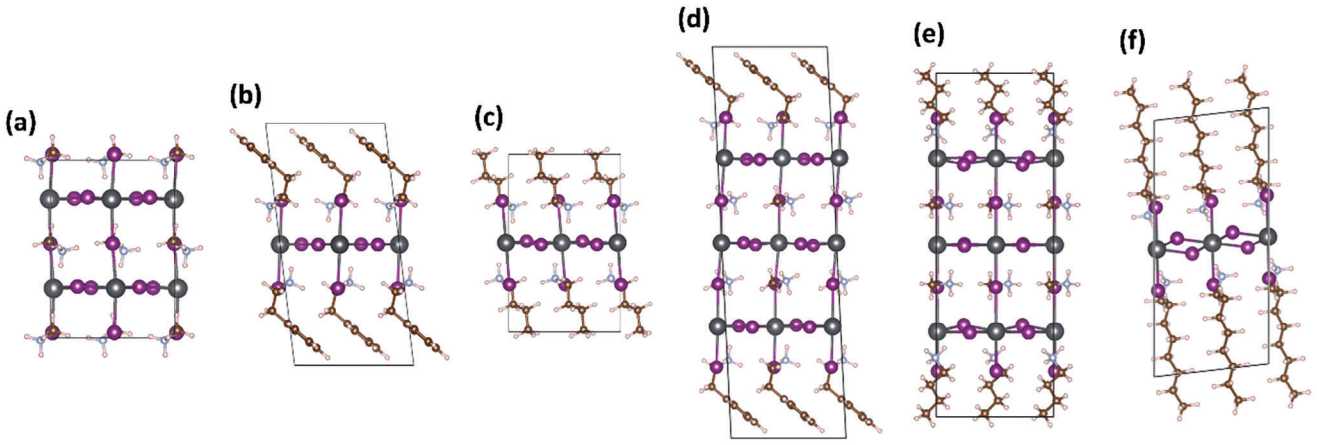

Figure 1. Investigated structures in this study; a) $MAPbI_3$, b) PEA_2PbI_4, c) BA_2PbI_4, d) $(PEA)_2(MA)_2Pb_3I_{10}$, e) $(BA)_2(MA)_2Pb_3I_{10}$, and f) $OCTA_2PbI_4$.

HC population (≈100 ps) was further revealed.[9–12] Various mechanisms with a possible interplay have been proposed for explaining the HC cooling process, including i) Auger heating effect; ii) large polaron screening effect;[13] iii) hot phonon bottleneck effect[9] depending on the carrier concentration.[4] Auger-heating or inter-band Auger recombination processes involve the non-radiative transfer of the electron–hole recombination energy to another carrier resulting in excitation of this carrier to a higher energetic state approximately equal to the bandgap energy, thus heating the electronic system and slowing down the carrier dynamics.[14,15] The formation of polarons, on the other hand, may slow down the cooling process by confining the charge carrier in the polarized potential cloud of the surrounding ions. Such polaron cloud extends up to several unit cells and forms "large polaron" in 3D perovskites.[16–20] The presence of lattice defects, variation in the chemical composition or quantum confinement in lower dimensional perovskites, may lead to a further spatial localization with the formation of "small polarons",[21–24] extending up to few atomic centers. The third mechanism, i.e., the phonon bottleneck effect, refers to the slowing down of the cooling process at high carrier density due to the presence of a large number of non-equilibrium longitudinal optical (LO) phonon population, resulting in the net reduction of LO phonon emission with a concomitant effect of slow HC cooling.[15,25,26] Acoustic-optical phonon up-conversion, i.e., the up-transition of low-energy modes through the overlapping phonon branches has also been credited as a reason of hot bottleneck effect.[27]

In this context, the hypothesis crediting the phonon gap between optical and acoustic branches has also been demonstrated as a reason of slow cooling of the HC of $MAPbI_3$,[15,28] following Klemens or Ridley mechanism as observed in pure inorganic semiconductors like InP and nanostructured GaAs.[29,30] In a quite similar argument, some authors have proposed the presence of phonon gap between optical and acoustic modes in $MAPbI_3$ by considering the major optical branches generated by the inorganic moiety[15]; however in a contradictory argument,[27] the motion of the organic sub-lattice also generates optical phonons by coupling with inorganic sub-lattice and can eventually create a continuum in the phonon density of states (DOS). The absence of persistent HC in the all-inorganic $CsPbBr_3$ perovskite further supports the claim that the organic sub-lattice coupled with inorganic sub-lattice may also contribute to the active optical modes.[10] Therefore, the mechanism of HC cooling is still controversial and under debate.

HC dynamics becomes even more complex and interesting in 2D/3D perovskites. Pure 2D perovskites share the same corner-sharing octahedral framework of 3D perovskites, but the inorganic layers are separated by large organic cations and form quantum well structures. 2D/3D perovskites are described by the formula $A_2B_{n-1}M_nX_{3n+1}$, where A is large cation, B is small cations, M is metal, and X is halide and n determines the number of inorganic layers, which reduces to a pure 2D case when $n = 1$. The high exciton binding energy due to quantum and dielectric confinement,[31–34] the strong optical transition strengths due to the dipole orientation of large cations,[35,36] and the occurrence of small polaron associated to self-trapped carriers[21,37–39] make carrier relaxation in 2D perovskites more complex than in its 3D counterpart.[40] Several works highlighted that HC cooling becomes faster in 2D perovskites compared to their 3D counterpart, by showing an intermediate behavior for 2D/3D perovskites endowed with more than a single inorganic layer in the quantum well.[41–47]

Despite the significant number of experimental works investigating HC relaxation time scales, a clear picture of the possible mechanisms behind the different cooling rates in 3D and 2D perovskites is still missing. In this work, we investigate the e-ph interaction and its influence on the HC cooling process in the 2D prototype perovskites $(BA)_2(MA)_{n-1}Pb_nI_{3n+1}$ and $(PEA)_2(MA)_{n-1}Pb_nI_{3n+1}$ (BA = n-butylammonium, PEA = phenylethylammonium, and MA = methylammonium) with $n = 1$, 3, by doing a direct comparison with 3D $MAPbI_3$. For simplicity, we refer to the $(BA)_2(MA)_{n-1}Pb_nI_{3n+1}$ with $n = 1$ and $n = 3$ henceforth as BA-n1 and BA-n3, respectively. Similarly, $(PEA)_2(MA)_{n-1}Pb_nI_{3n+1}$ with $n = 1$ and $n = 3$ are referred henceforth as PEA-n1 and PEA-n3, respectively, see **Figure 1**.

Our study shows that while in $MAPbI_3$ e-ph coupling is dominated by the low-frequency (<60 cm^{-1}) Pb—I bending phonon modes, in 2D perovskites higher-frequency phonon modes (60–120 cm^{-1}) associated to the stretching of the inorganic sublattice introduce additional e-ph scattering, by increasing the HC's cooling rate. The e-ph coupling with high-frequency phonon

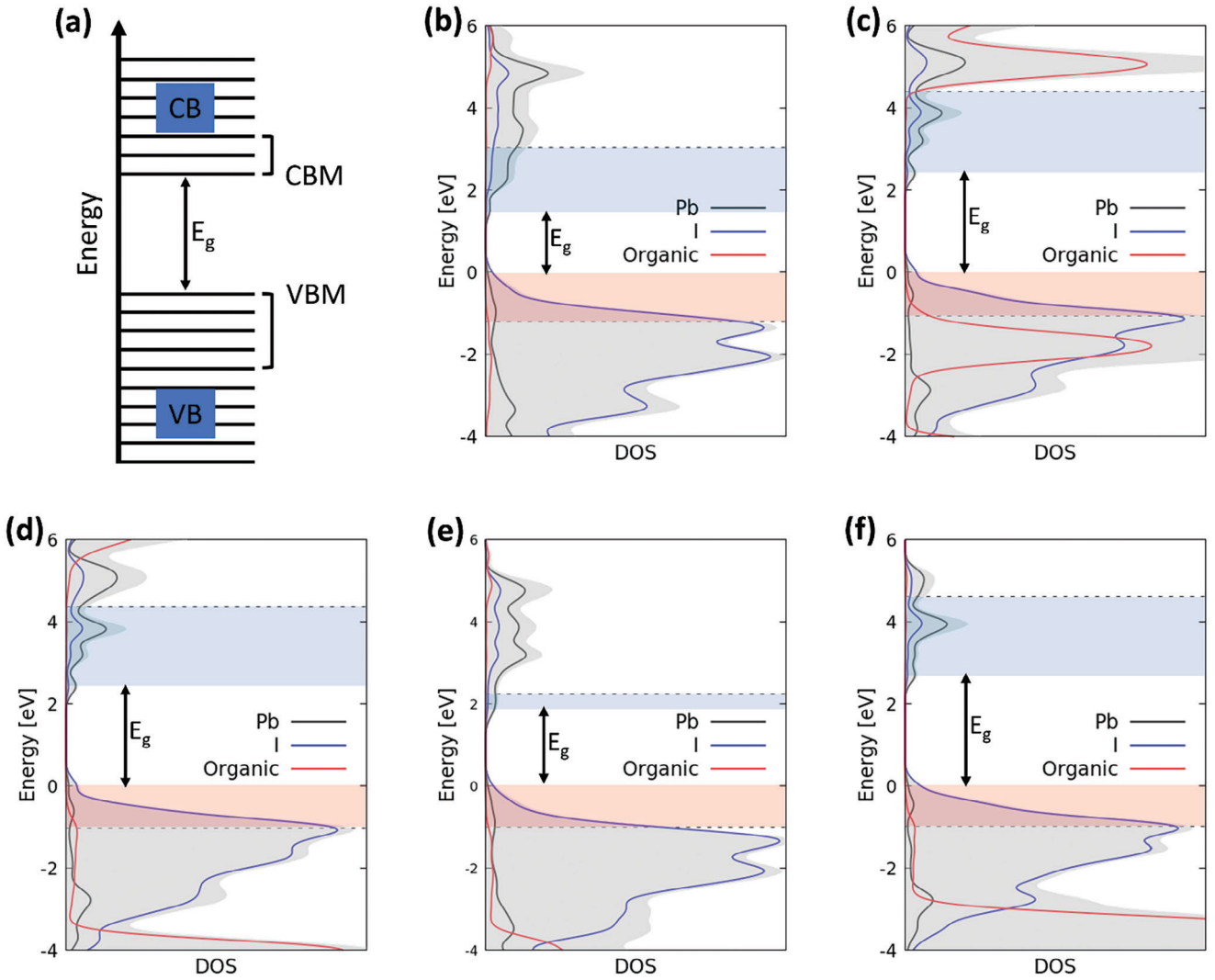

Figure 2. a) Schematic representation of the VB and CB electronic states included in the e-ph coupling analysis at the Γ point. Electronic DOS of b) $MAPbI_3$, c) PEA_2PbI_4, d) BA_2PbI_4, e) $(BA)_2(MA)_2Pb_3I_{10}$, and f) $OCTA_2PbI_4$. The energy range spanned by VB and CB states for the hot hole and electron analysis are indicated by red and blue area, respectively, in the different cases. The energy range spans up to 1.20 (1.49), 1.07 (1.99), 1.04 (1.93), 1.00 (0.45), and 0.99 (1.93) eV for the VB (CB) bands for $MAPbI_3$, PEA_2PbI_4, BA_2PbI_4, $(BA)_2(MA)_2Pb_3I_{10}$, and $OCTA_2PbI_4$, respectively.

modes in 2D perovskites decreases by increasing the quantum well thickness of the inorganics, while it only slightly depends upon the organic spacer length, indicating that the e-ph coupling is strongly modulated by the quantum confinement in the inorganic sublattice.

2. Results and Discussion

E-ph interaction of each phonon mode with the Kohn-Sham states of the different investigated systems has been investigated by calculating the e-ph relaxation energy (λ), defined by the following expression[28,48–51]

$$\lambda_i = \left(\frac{dE}{dQ_i}\right)^2 \left(\frac{1}{2\alpha_i}\right) \quad (1)$$

where dE is the shift in the KS orbital energy upon the i-th phonon perturbation, dQ_i is the displacement of the lattice associated with the i-th phonon mode and α_i is the curvature of the potential energy surface along the i-th phonon mode. Such an approach has been widely adopted to investigate e-ph processes in metal halide perovskites,[50] providing results in good agreement with both experiments[50] and different methods.[52,53] E-ph coupling is calculated by considering couplings between the electronic states and the phonons at the Γ point in the Brillouin zone (BZ). This approach is justified by the evidence that for $MAPbI_3$ e-ph coupling with phonons at different high symmetry q-points across the BZ have very limited contributions (<8 meV), as illustrated in Figure S1 (Supporting Information). Furthermore, to accurately determine the electronic response to phonon deformation, single point calculations along the phonon displacements have been performed with the hybrid HSE06 functional by including spin-orbit coupling (SOC), see additional

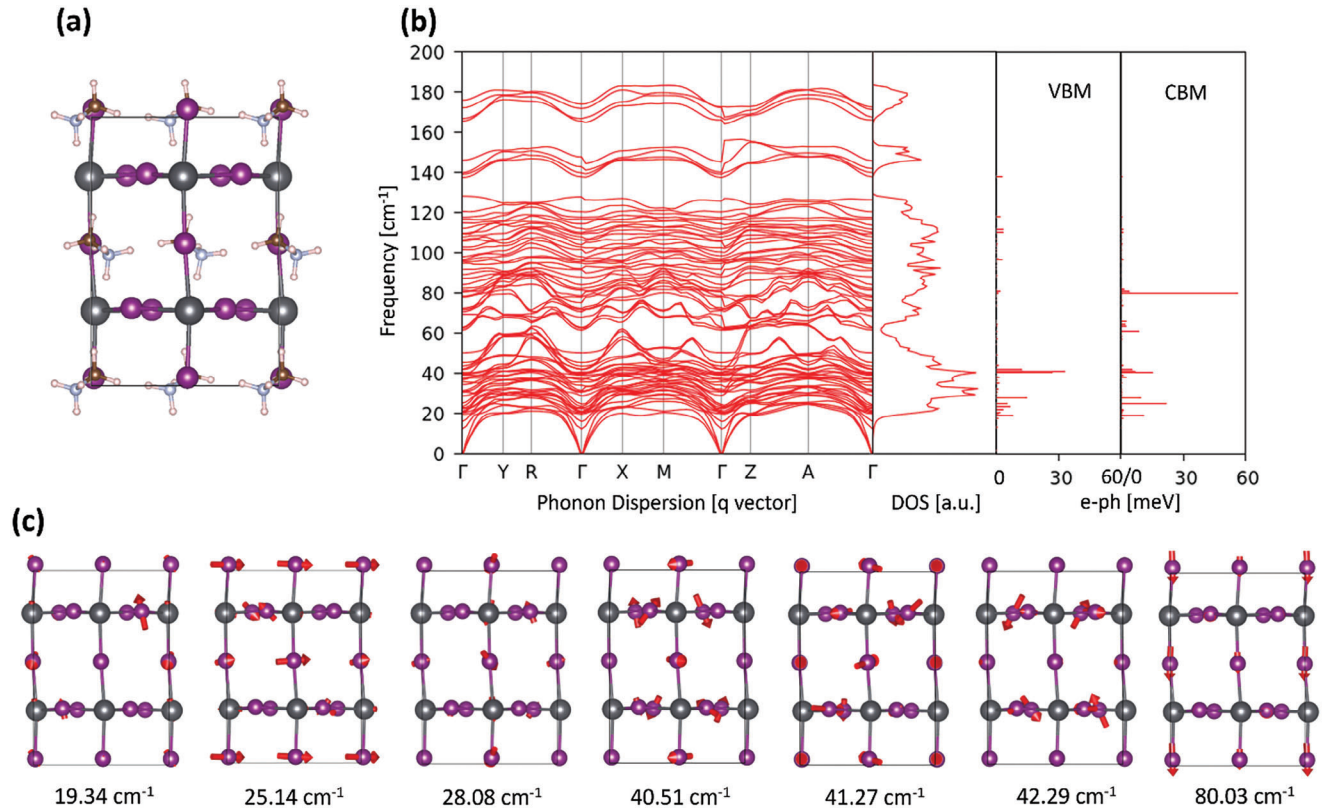

Figure 3. a) Optimized structure and b) phonon dispersion, phonon DOS across the whole Brillouin zone, and e-ph relaxation energies of VBM and CBM at Γ point of tetragonal $MAPbI_3$. c) phonon modes with significant e-ph interaction at Γ q-point; organic cations have been removed for the clarity. e-ph coupling at the third and fourth panels of (b) represents the coupling associated with the VBM and CBM; e-ph coupling for the higher energy bands are shown in Table 1 and Tables S1 and S2 (Supporting Information).

Computational details in Supporting Information and Figure S2 (Supporting Information) for a comparison with GGA results. For mapping the HC cooling, the e-ph coupling at the Γ point has been investigated for six valence band (VB) states, including valence band maximum VBM (≈1.0 eV energy window for all the phases), and three conduction bands (CB) states, including conduction band minimum CBM (≈1.5, 2.0, and 0.5 eV energy window for 3D, 2D, and 2D-n3 phases, respectively), see **Figure 2**. Such approach makes our analysis independent from the bandgaps of the considered phases. Due to the large n3 systems size, HSE06-SOC e-ph coupling have been calculated only for BA-n3. However, the phonon analysis has been performed in PEA-n3 and the resemblance of phonon DOS and nature of vibrations (Figure S3, Supporting Information) with that of BA-n3 suggests that the PEA-n3 and BA-n3 might show similar e-ph coupling trend.

We start by analyzing the results for the prototype $MAPbI_3$ in its room temperature stable tetragonal phase. Phonon band structures, phonon DOS and the e-ph relaxation energies of VBM and CBM levels with each phonon mode at Γ are shown in **Figure 3**. As one can see from Figure S4 (Supporting Information), the atomic displacements due to Pb—I bond vibrations and the associated e-ph coupling extend up to 170 cm^{-1}. Since the electronic states of the organic cations are not directly coupled to band edge states and atomic displacements of inorganic atoms do not extend above 200 cm^{-1}, we have focused into the phonon modes up to 200 cm^{-1}. Within this frequency range, the phonon frequencies have been subdivided in three regions based on the different nature of the vibrations, i.e., below 60 cm^{-1} where mainly Pb—I bending modes are present, between 60 and 120 cm^{-1} with phonons associated to stretching of the inorganics, and above 120 cm^{-1} associated to the bending and stretching of the large organic cations.

As can be seen in Figure 3b, the strongest e-ph couplings for the VBM and CBM levels are mainly originated from the Pb—I bending motions at 19.34, 25.14, 28.08, 40.51, 41.27, and 42.29 cm^{-1} and one mode from the axial Pb—I stretching vibration (80.03 cm^{-1}), in agreement with previous literature.[52,54]

The cumulative relaxation energy, i.e., the sum of the calculated relaxation energies over the normal modes in each frequency range of the six VB and three CB states delimiting red and blue areas in Figure 2b are summarized in **Table 1** (details of e-ph coupling for each band are reported in Tables S1 and S2, Supporting Information). Cumulative relaxation energies confirm that a significant contribution of e-ph interaction for VB states appears below <60 cm^{-1} whereas both the <60 and 60–120 cm^{-1} regions are populated for the CB states.

We now move to investigate e-ph coupling in 2D/3D perovskites. In **Figure 4** the phonon DOS, the relaxation energies of the VBM and CBM are reported, while in Table 1 the cumulative e-ph coupling of VB and CB states in the three frequency regions are reported.

Table 1. Cumulative e-ph coupling in the different frequency regions for the various systems. For each system the cumulative e-ph coupling between Γ phonon modes and the VB and CB states in the red and blue areas in Figure 2 are reported. The detailed values for each energy band are provided in Tables S1 and S2 (Supporting Information).

Systems		Cumulative relaxation energies λ (meV) in the different frequency regions		
		0–60 cm^{-1}	60-120 cm^{-1}	120–200 cm^{-1}
$MAPbI_3$	VBs	310	148	52
Eg = 1.54 eV	CBs	140	142	0
PEA_2PbI_4	VBs	318	774	8
Eg = 2.41 eV	CBs	178	1272	0
BA_2PbI_4	VBs	266	1112	42
Eg = 2.43 eV	CBs	138	1710	12
$(BA)_2(MA)_2Pb_3I_{10}$	VBs	352	308	118
Eg = 1.79 eV	CBs	226	286	34
$OCTA_2PbI_4$	VBs	344	620	0
Eg = 2.69 eV	CBs	184	756	0

By comparing stretching phonon modes of the Pb—I bonds of $MAPbI_3$ and, e.g., BA-n1 (see Figures 3b and 4b) the normal modes appear at almost similar frequencies, with axial Pb—I stretching at 80.03, 111.94, and 118.07 cm^{-1} for $MAPbI_3$, 75.66 and 79.21 cm^{-1} for BA-n1, 75.92, and 79.91 cm^{-1} for PEA-n1; equatorial Pb—I stretching at 96.79 and 110.55 cm^{-1} for $MAPbI_3$, 72.42, 97.58 and 109.26 cm^{-1} for BA-n1, 78.73, 99.75, and 108.91 cm^{-1} for PEA-n1. The slightly lower value of axial Pb—I stretching peaks of BA-n1 than $MAPbI_3$ is justified since the axial iodine atoms are under-coordinated in BA-n1.

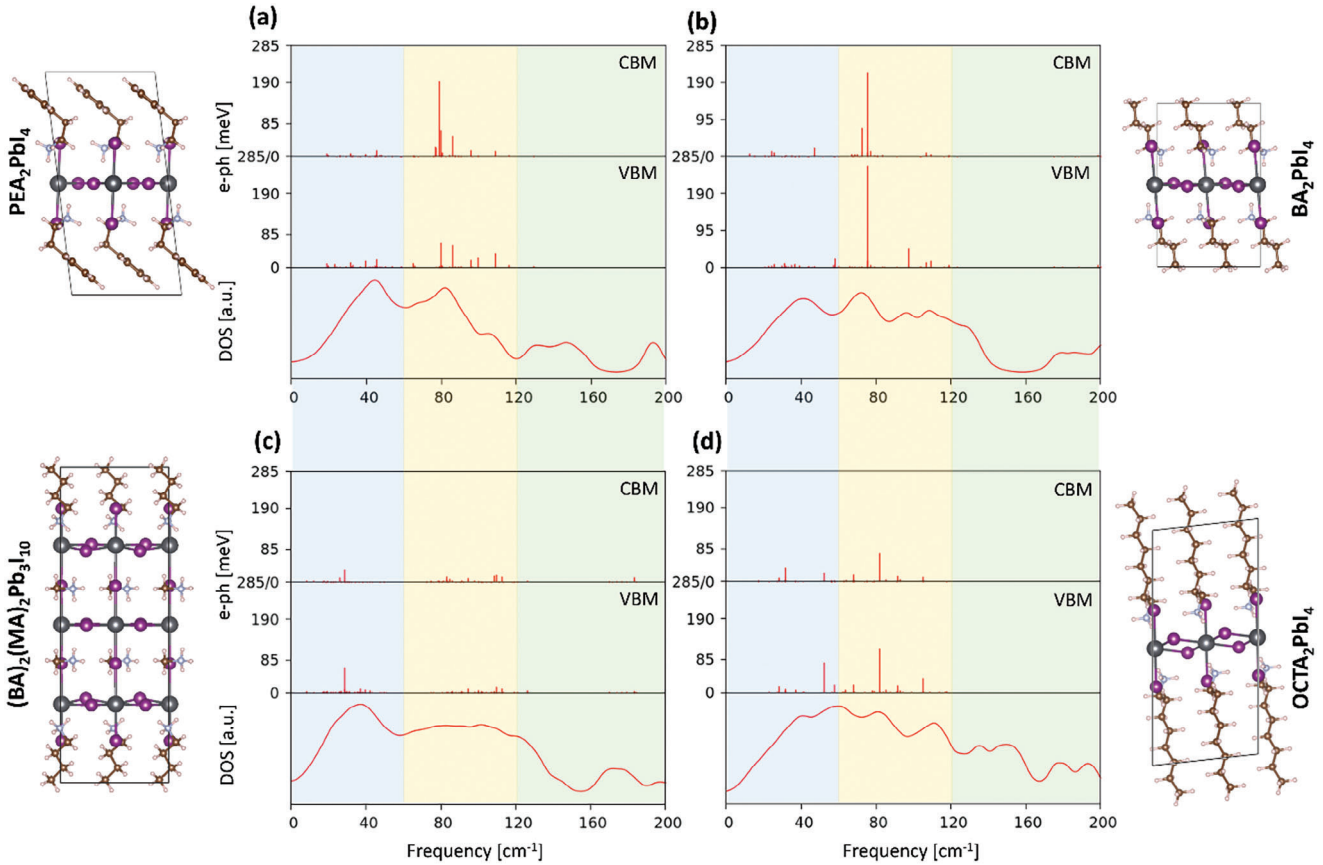

Figure 4. Optimized structures, phonon DOS and e-ph relaxation energies of VBM and CBM of a) PEA-n1, b) BA-n1, c) BA-n3, and d) OCTA-n1. Phonon DOS are reported for Γ q-point. Transparent blue, yellow and green regions represent region-1, region-2, and region-3, respectively.

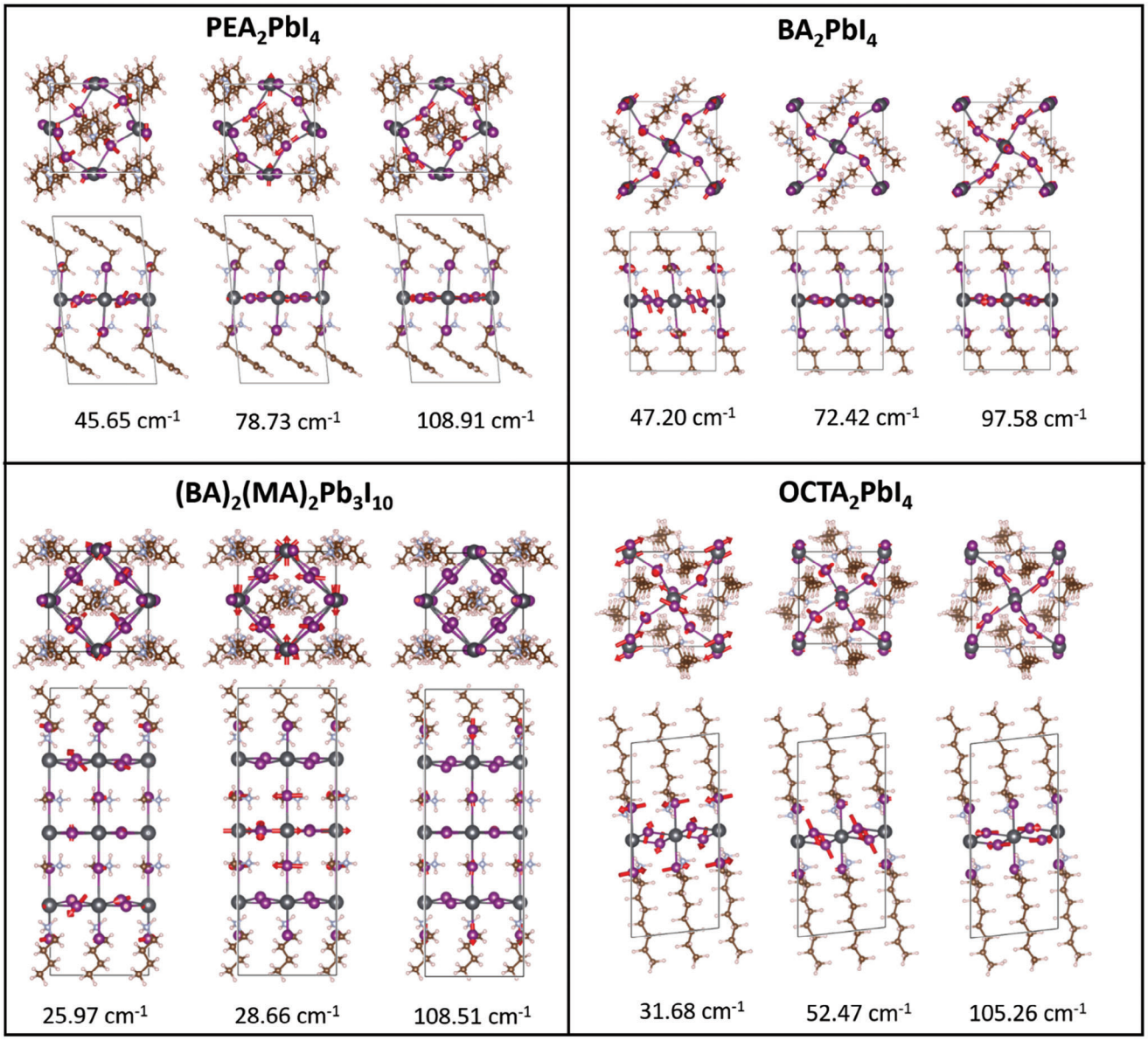

Figure 5. Displacement vectors of the phonon modes with significant e-ph coupling at the band edges at the region-1 and region-2 for PEA-n1, BA-n1, BA-n3, and OCTA-n1 structures. Displacements vectors for the organic cations have been removed for clarity.

Interestingly, for PEA-n1 and BA-n1, e-ph coupling shows an increased contribution from the high-frequency region-2 branch (60–120 cm^{-1}) compared to region-1 branch (<60 cm^{-1}), see Figure 4 and Table 1. The highest e-ph interactions in energy region-2 are mainly associated to axial and equatorial stretching of the inorganics, see **Figure 5**, and show absolute relaxation energies remarkably higher than those calculated in the 3D $MAPbI_3$ perovskite.

From this analysis a clear trend is emerging, i.e., moving from 3D to 2D perovskites stretching phonons belonging to the higher frequency region-2 (60–120 cm^{-1}) start to dominate the e-ph coupling. Notably, equatorial stretching modes above 80 cm^{-1} are not coupled to electronic states in $MAPbI_3$. Since inorganic moiety's vibrations are very much similar in $MAPbI_3$ and BA-n1, the absence of strong e-ph peaks for $MAPbI_3$ in region-2 may be ascribed to the more sensitive response of the quantum confined 2D-inorganics to in-plane stretching modes with respect to the 3D periodic bulk system, as has been depicted from the wave function plots of the normal modes for 3D and 2D systems in **Figure 6**.

The impact of structural factors, specifically the thickness of the inorganic layer and the length of the large cations, on the electronic response to phonon displacement, i.e., the e-ph coupling strength, can be monitored by the analysis of e-ph coupling in BA-n3 and OCTA-n1 perovskites. By increasing the thickness of the inorganic layer to form the 2D-n3 perovskites, a progressive decrease of the e-ph relaxation energies at the band edges is reported in energy region-2, indicating a more limited coupling

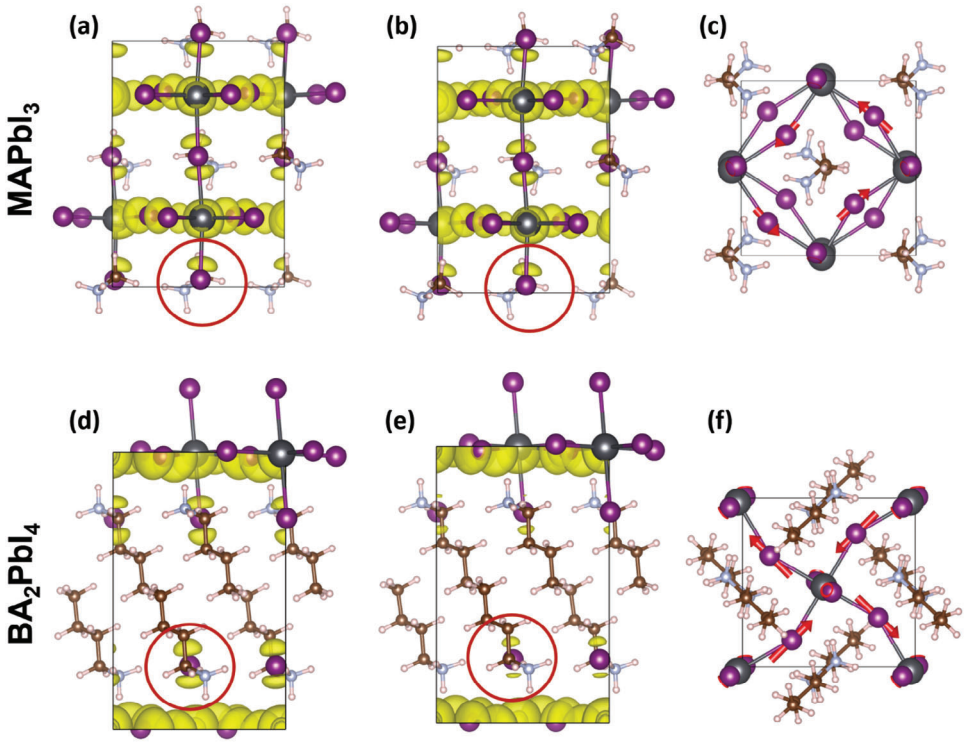

Figure 6. Wavefunction plots of the VBM Kohn-Sham levels of the $MAPbI_3$ and BA_2PbI_4 for the a,d) pristine structures b,e) normal modes structures and c,f) displacement vectors associated with in-plane stretching vibration of 96.79 and 97.58 cm^{-1} for $MAPbI_3$ and BA_2PbI_4, respectively. Highlighted parts indicate that, for the similar kind of vibration of the inorganic atoms, the charge density remain similar in $MAPbI_3$, whereas it gets modulated significantly in BA_2PbI_4. Isosurface values of the pristine and normal modes structures have been maintained similar for proper comparison; 0.0008 and 0.0006 e $Å^{-3}$ for $MAPbI_3$ and BA_2PbI_4, respectively. Displacements vectors for the organic cations have been removed for clarity for both $MAPbI_3$ and BA_2PbI_4.

of the bulk-like n3 system with Pb—I stretching. Absolute e-ph values are calculated in between 3D and 2D systems and the cumulative e-ph coupling distribution spreads back region-1.

The effect of the organic spacer length, i.e., the different electronic coupling between the inorganic layers, has instead a more limited impact. As can be seen from Table 1, for $OCTA_2PbI_4$ (henceforth as OCTA-n1) the e-ph coupling strength is comparable to PEA-n1 and BA-n1 perovskites, even though a limited variation in e-ph coupling distribution between region-1 and region-2 is observed for OCTA-n1. Notably, di-ammonium cations as in the Dion Jacobson perovskites[55–57] may show a different behavior with respect to mono-ammonium cation by bringing additional rigidity and eventually decreasing the e-ph coupling.

These results show that quantum confinement of the charge carriers is the primary factor modulating e-ph coupling in these systems. The e-ph response decreases almost linearly with increasing thickness of the inorganic layer, associated to an increased coupling of the electronic states with Pb—I bending modes which dominate e-ph coupling in bulk 3D systems.

Based on e-ph coupling analysis, the origin of the different HC cooling rates in 3D and 2D perovskites can be hypothesized. Immediately after photoexcitation with above bandgap energy, HC start relaxing via carrier-phonon interactions, as depicted in **Scheme 1**. The larger the carrier-phonon interaction, the faster is the HC relaxation toward the band edges.

In turn, the larger is the population in the high-frequency phonons (in region-2 or region-3), the higher is the number of phonon scattering channels and e-ph scattering rate;[58,59] consequently the faster HC cooling becomes. Alongside, if an increased number of low-frequency phonons (in region-1) are activated, a higher number of phonons has to be emitted compared to high-frequency phonons in order to cool down the same excess energy.[15,30] Therefore, summing up the characteristics of the e-ph mediated HC decay process, it emerges that the higher is the fractional ratio of e-ph population in the region-1 the slower will HC cooling be.

As reported before, e-ph coupling is driven by the scattering with low-frequency phonons (in region-1) for $MAPbI_3$, whereas high-frequency region-2 dominates for 2D perovskites. The stronger coupling in the frequency region-2 indicates that HC cooling is faster in 2D perovskites with $n = 1$, approaching the bulk limit when increasing the number of inorganic layers, as discussed for systems with $n = 3$. Experimental evidences on the time scale of HC cooling nicely match with the outcome of our analysis. While the e-ph interaction is probed by the full width half maximum (FWHM) of the broad luminescence behavior,[60–65] the HC dynamics have been studied by monitoring the high-energy tail and decay characteristic of time-resolved photoluminescence (TRPL) and transient absorption (TA) spectra.[8,10,66,67] The fast component decay in the picosecond scale typically arises due to carrier thermalization and

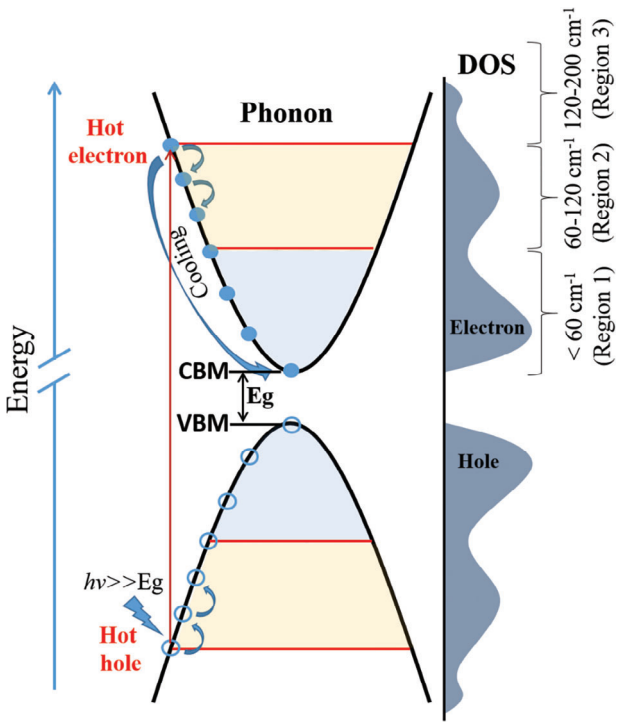

Scheme 1. Schematic representation of the excitation and cooling process of the HC. Phonon DOS has been schematically quantified in different regions based on the different nature of vibrations of the metal-halide bonds of metal-halide perovskites class of materials.

HC cooling; thus a faster decay of the "fast component" of TRPL and TA dynamics implies a higher e-ph interaction.[68,69] Cho et al.,[47] from the bi-exponential kinetic fitting of the time-resolved TA spectra, reported the increased contribution of short lifetime component with decreasing the value of n in $(PEA)_2MA_{n-1}Pb_nI_{3n+1}$ structures. Hintermayr et al.[70] reported a time constant of 1.7 ps carriers cooling in quasi-3D $MAPbI_3$ nanoplatelets, while in the 2D counterpart the time constant is 0.24 ps. Additionally Maity et al.,[45] by studying coherent longitudinal acoustic phonons' propagation from femtosecond transient reflectance spectroscopy, reported slower HC cooling by increasing the layer number from $n = 1$ to $n = 3$ in $(PEA)_2MA_{n-1}Pb_nI_{3n+1}$ structures.

As a final remark, the polaron nature of charge carriers is expected to play a role in the HC cooling process.[13,19,20] Irrespective of whether hole or electron polarons are considered, it is clear that polaron size start becoming "large" with the decrease of quantum confinement, as has been shown in Figures S5 and S6 (Supporting Information). As proposed by Zhu and co-workers,[13,19] large polaron can further contribute to decrease the HC cooling by increasing the screening ability of the carriers in 3D and PEA-n3 and BA-n3 perovskites.

Our analysis elucidated the e-ph coupling trend by moving from the 3D to 2D perovskites, i.e., by increasing the quantum confinement of the inorganic subunit. A topic of emerging interest is represented by the e-ph coupling in mixed 3D/2D perovskite hetero-structures. The coupling of 2D and 3D perovskites in 2D/3D architectures is a promising strategy to increase the long term stability of devices. Due to the higher complexity of the system, the effects of the interface on the charge carrier cooling rate cannot be easily extrapolated from our results in 3D and 2D single units. While an intermediate cooling rate between the 3D and 2D limit cases can be expected, lattice mismatch and charge transfer at the interface[33,71–75] can profoundly alter the e-ph coupling behavior. Furthermore, the presence of partially saturated interfacial bonds and defects at the interface can emerge as the major cooling channels in these systems.

3. Conclusion

In summary, our high-level calculations highlight a competition of e-ph coupling between the bending and stretching phonon branches, differentiating the HC cooling behavior in 3D and 2D perovskites. e-ph coupling of 3D perovskites is dominated by low-frequency bending phonon branches, whereas high-frequency stretching phonon modes dominate $n = 1$ 2D systems. The increased e-ph coupling strength in 2D perovskites is in agreement with the faster HC cooling process in 2D perovskites. Inorganic layer thickness, modulating the quantum confinement in 2D perovskites, is the primary factor determining the e-ph coupling in the systems, while the length of the spacer cations only slightly influences the e-ph interaction. Larger screening associated to large polarons may further contribute to slow down HC in 3D perovskite. This study contributes to unveil the origin of the experimental observation of HC cooling trends in 3D and 2D perovskites and provides a route map for tuning the e-ph interaction, which is key for utilizing the HC and consequently overcoming the Shockley-Queisser limit of conversion efficiency.

Supporting Information

Supporting Information is available from the Wiley Online Library or from the author.

Acknowledgements

This study was developed in the framework of the research activities carried out within the Project "Network 4 Energy Sustainable Transition—NEST", Spoke 1, Project code PE0000021, funded under the National Recovery and Resilience Plan (NRRP), Mission 4, Component 2, Investment 1.3— Call for tender No. 1561 of 11.10.2022 of Ministero dell'Universitaé della Ricerca (MUR); funded by the European Union—NextGenerationEU. This work has been also funded by the European Union - NextGenerationEU under the Italian Ministry of University and Research (MUR) National Innovation Ecosystem grant ECS00000041 - VITALITY - CUP: J97G22000170005 and CUP: B43C22000470005. The authors acknowledge Università degli Studi di Perugia and MUR for support within the project Vitality. D.M. and S.F. acknowledge the European Union's Horizon Europe research and innovation program under grant agreement no. 101082176 – VALHALLA. A.M. acknowledges the seed grant (SG/IITH/F301/2022-23/SG-145) from IIT Hyderabad for financial support.

Conflict of Interest

The authors declare no conflict of interest.

Data Availability Statement

The data that support the findings of this study are available in the supplementary material of this article.

Keywords

electron–phonon coupling, hot carrier cooling, metal-halide perovskites, perovskites solar cell

Received: October 9, 2023
Revised: November 25, 2023
Published online:

[1] M. A. Green, A. Ho-Baillie, H. J. Snaith, *Nat. Photonics* **2014**, *8*, 506.
[2] A. Kojima, K. Teshima, Y. Shirai, T. Miyasaka, *J. Am. Chem. Soc.* **2009**, *131*, 6050.
[3] A. J. Nozik, *Annu. Rev. Phys. Chem.* **2001**, *52*, 193.
[4] M. Li, J. Fu, Q. Xu, T. C. Sum, *Adv. Mater.* **2019**, *31*, 1802486.
[5] Z. Guo, Y. Wan, M. Yang, J. Snaider, K. Zhu, L. Huang, *Science* **2017**, *356*, 59.
[6] J. M. Frost, L. D. Whalley, A. Walsh, *ACS Energy Lett.* **2017**, *2*, 2647.
[7] R. T. Ross, A. J. Nozik, *J. Appl. Phys.* **1982**, *53*, 3813.
[8] G. Xing, N. Mathews, S. Sun, S. S. Lim, Y. M. Lam, M. Grätzel, S. Mhaisalkar, T. C. Sum, *Science* **2013**, *342*, 344.
[9] Y. Yang, D. P. Ostrowski, R. M. France, K. Zhu, J. Van De Lagemaat, J. M. Luther, M. C. Beard, *Nat. Photonics* **2015**, *10*, 53.
[10] H. Zhu, K. Miyata, Y. Fu, J. Wang, P. P. Joshi, D. Niesner, K. W. Williams, S. Jin, X.-Y. Zhu, *Science* **2016**, *353*, 1409.
[11] D. Niesner, H. Zhu, K. Miyata, P. P. Joshi, T. J. S. Evans, B. J. Kudisch, M. T. Trinh, M. Marks, X.-Y. Zhu, *J. Am. Chem. Soc.* **2016**, *138*, 15717.
[12] M. Li, S. Bhaumik, T. W. Goh, M. S. Kumar, N. Yantara, M. Grätzel, S. Mhaisalkar, N. Mathews, T. C. Sum, *Nat. Commun.* **2017**, *8*, 14350.
[13] X.-Y. Zhu, V. Podzorov, *J. Phys. Chem. Lett.* **2015**, *6*, 4758.
[14] M. Achermann, A. P. Bartko, J. A. Hollingsworth, V. I. Klimov, *Nat. Phys.* **2006**, *2*, 557.
[15] J. Fu, Q. Xu, G. Han, B. Wu, C. H. A. Huan, M. L. Leek, T. C. Sum, *Nat. Commun.* **2017**, *8*, 1300.
[16] K. Miyata, D. Meggiolaro, M. T. Trinh, P. P. Joshi, E. Mosconi, S. C. Jones, F. De Angelis, X.-Y. Zhu, *Sci. Adv.* **2017**, *3*, 1701217.
[17] F. Ambrosio, J. Wiktor, F. De Angelis, A. Pasquarello, *Energy Environ. Sci.* **2018**, *11*, 101.
[18] F. Zheng, L.-W. Wang, *Energy Environ. Sci.* **2019**, *12*, 1219.
[19] K. Miyata, D. Meggiolaro, M. T. Trinh, P. P. Joshi, E. Mosconi, S. C. Jones, F. De Angelis, X.-Y. Zhu, *Sci. Adv.* **2017**, *3*, 1701217.
[20] D. Meggiolaro, F. Ambrosio, E. Mosconi, A. Mahata, F. De Angelis, *Adv. Energy Mater.* **2019**, *10*, 1902748.
[21] D. Cortecchia, J. Yin, A. Bruno, S.-Z. A. Lo, G. G. Gurzadyan, S. Mhaisalkar, J.-L. Brédas, C. Soci, *J. Mater. Chem. C* **2017**, *5*, 2771.
[22] J. Yin, P. Maity, M. De Bastiani, I. Dursun, O. M. Bakr, J.-L. Brédas, O. F. Mohammed, *Sci. Adv.* **2017**, *3*, 1701793.
[23] A. Mahata, D. Meggiolaro, F. De Angelis, *J. Phys. Chem. Lett.* **2019**, *10*, 1790.
[24] A. J. Neukirch, I. I. Abate, L. Zhou, W. Nie, H. Tsai, L. Pedesseau, J. Even, J. J. Crochet, A. D. Mohite, C. Katan, S. Tretiak, *J. Phys. Chem. Lett.* **2018**, *9*, 7130.
[25] J. R. Senna, S. Das Sarma, *Solid State Commun.* **1987**, *64*, 1397.
[26] J. M. Richter, F. Branchi, F. Valduga De Almeida Camargo, B. Zhao, R. H. Friend, G. Cerullo, F. Deschler, *Nat. Commun.* **2017**, *8*, 376.
[27] J. Yang, X. Wen, H. Xia, R. Sheng, Q. Ma, J. Kim, P. Tapping, T. Harada, T. W. Kee, F. Huang, Y.-B. Cheng, M. Green, A. Ho-Baillie, S. Huang, S. Shrestha, R. Patterson, G. Conibeer, *Nat. Commun.* **2017**, *8*, 14120.
[28] S. D. Verma, Q. Gu, A. Sadhanala, V. Venugopalan, A. Rao, *ACS Energy Lett.* **2019**, *4*, 736.
[29] Y. Zhang, X. Jia, S. Liu, B. Zhang, K. Lin, J. Zhang, G. Conibeer, *Sol. Energy Mater. Sol. Cells* **2021**, *225*, 111073.
[30] S. Kahmann, M. A. Loi, *J. Mater. Chem. C* **2019**, *7*, 2471.
[31] X. Hong, T. Ishihara, A. V. Nurmikko, *Phys. Rev. B* **1992**, *45*, 6961.
[32] H. Tsai, W. Nie, J.-C. Blancon, C. C. Stoumpos, R. Asadpour, B. Harutyunyan, A. J. Neukirch, R. Verduzco, J. J. Crochet, S. Tretiak, L. Pedesseau, J. Even, M. A. Alam, G. Gupta, J. Lou, P. M. Ajayan, M. J. Bedzyk, M. G. Kanatzidis, A. D. Mohite, *Nature* **2016**, *536*, 312.
[33] A. Mahata, E. Mosconi, D. Meggiolaro, F. De Angelis, *Chem. Mater.* **2020**, *32*, 105.
[34] C. Katan, N. Mercier, J. Even, *Chem. Rev.* **2019**, *119*, 3140.
[35] A. H. Proppe, G. W. Walters, A. Y. Alsalloum, A. A. Zhumekenov, E. Mosconi, S. O. Kelley, F. De Angelis, L. Adamska, P. Umari, O. M. Bakr, E. H. Sargent, *J. Phys. Chem. Lett.* **2020**, *11*, 716.
[36] W. Liu, J. Xing, J. Zhao, X. Wen, K. Wang, P. Lu, Q. Xiong, *Adv. Opt. Mater.* **2017**, *5*, 1601045.
[37] J. Yin, H. Li, D. Cortecchia, C. Soci, J.-L. Brédas, *ACS Energy Lett.* **2017**, *2*, 417.
[38] R. Gautier, M. Paris, F. Massuyeau, *J. Am. Chem. Soc.* **2019**, *141*, 12619.
[39] D. B. Straus, C. R. Kagan, *J. Phys. Chem. Lett.* **2018**, *9*, 1434.
[40] K. Zheng, T. Pullerits, *J. Phys. Chem. Lett.* **2019**, *10*, 5881.
[41] P. Guo, C. C. Stoumpos, L. Mao, S. Sadasivam, J. B. Ketterson, P. Darancet, M. G. Kanatzidis, R. D. Schaller, *Nat. Commun.* **2018**, *9*, 2019.
[42] X. Jia, J. Jiang, Y. Zhang, J. Qiu, S. Wang, Z. Chen, N. Yuan, J. Ding, *Appl. Phys. Lett.* **2018**, *112*, 143903.
[43] Z. Guo, X. Wu, T. Zhu, X. Zhu, L. Huang, *ACS Nano* **2016**, *10*, 9992.
[44] S.-F. Zhang, X.-K. Chen, A.-M. Ren, H. Li, J.-L. Bredas, *ACS Energy Lett.* **2019**, *4*, 17.
[45] P. Maity, J. Yin, B. Cheng, J.-H. He, O. M. Bakr, O. F. Mohammed, *J. Phys. Chem. Lett.* **2019**, *10*, 5259.
[46] Z. Zhang, W.-H. Fang, M. V. Tokina, R. Long, O. V. Prezhdo, *Nano Lett.* **2018**, *18*, 2459.
[47] J. Cho, J. T. Dubose, P. V. Kamat, *J. Phys. Chem. Lett.* **2020**, *11*, 2570.
[48] X. Gong, O. Voznyy, A. Jain, W. Liu, R. Sabatini, Z. Piontkowski, G. Walters, G. Bappi, S. Nokhrin, O. Bushuyev, M. Yuan, R. Comin, D. Mccamant, S. O. Kelley, E. H. Sargent, *Nat. Mater.* **2018**, *17*, 550.
[49] Q. Du, C. Zhu, Z. Yin, G. Na, C. Cheng, Y. Han, N. Liu, X. Niu, H. Zhou, H. Chen, L. Zhang, S. Jin, Q. Chen, *ACS Nano* **2020**, *14*, 5806.
[50] F. Thouin, D. A. Valverde-Chávez, C. Quarti, D. Cortecchia, I. Bargigia, D. Beljonne, A. Petrozza, C. Silva, A. R. Srimath Kandada, *Nat. Mater.* **2019**, *18*, 349.
[51] L. Grisanti, Y. Olivier, L. Wang, S. Athanasopoulos, J. Cornil, D. Beljonne, *Phys. Rev. B* **2013**, *88*, 035450.
[52] S. Poncé, M. Schlipf, F. Giustino, *ACS Energy Lett.* **2019**, *4*, 456.
[53] F. Giustino, M. L. Cohen, S. G. Louie, *Phys. Rev. B* **2007**, *76*, 165108.
[54] A. D. Wright, C. Verdi, R. L. Milot, G. E. Eperon, M. A. Pérez-Osorio, H. J. Snaith, F. Giustino, M. B. Johnston, L. M. Herz, *Nat. Commun.* **2016**, *7*, 11755.
[55] D. Ghosh, D. Acharya, L. Pedesseau, C. Katan, J. Even, S. Tretiak, A. J. Neukirch, *J. Mater. Chem. A* **2020**, *8*, 22009.
[56] J. Yin, R. Naphade, P. Maity, L. Gutiérrez-Arzaluz, D. Almalawi, I. S. Roqan, J.-L. Brédas, O. M. Bakr, O. F. Mohammed, *Nat. Commun.* **2021**, *12*, 3995.
[57] J. Gong, M. Hao, Y. Zhang, M. Liu, Y. Zhou, *Angew. Chem., Int. Ed.* **2022**, *61*, 202112022.
[58] D. Zhao, H. Hu, R. Haselsberger, R. A. Marcus, M.-E. Michel-Beyerle, Y. M. Lam, J.-X. Zhu, C. La-O-Vorakiat, M. C. Beard, E. E. M. Chia, *ACS Nano* **2019**, *13*, 8826.
[59] M. C. Beard, G. M. Turner, C. A. Schmuttenmaer, *Phys. Rev. B* **2000**, *62*, 15764.
[60] H. Luo, S. Guo, Y. Zhang, K. Bu, H. Lin, Y. Wang, Y. Yin, D. Zhang, S. Jin, W. Zhang, W. Yang, B. Ma, X. Lü, *Adv. Sci.* **2021**, *8*, 2100786.
[61] S. Li, J. Luo, J. Liu, J. Tang, *J. Phys. Chem. Lett.* **2019**, *10*, 1999.
[62] S. Guo, Y. Zhao, K. Bu, Y. Fu, H. Luo, M. Chen, M. P. Hautzinger, Y. Wang, S. Jin, W. Yang, X. Lü, *Angew. Chem., Int. Ed.* **2020**, *59*, 17533.

[63] L. Ni, U. Huynh, A. Cheminal, T. H. Thomas, R. Shivanna, T. F. Hinrichsen, S. Ahmad, A. Sadhanala, A. Rao, *ACS Nano* **2017**, *11*, 10834.
[64] X. Lao, Z. Yang, Z. Su, Y. Bao, J. Zhang, X. Wang, X. Cui, M. Wang, X. Yao, S. Xu, *J. Phys. Chem. C* **2019**, *123*, 5128.
[65] X. Huang, X. Li, Y. Tao, S. Guo, J. Gu, H. Hong, Y. Yao, Y. Guan, Y. Gao, C. Li, X. Lü, Y. Fu, *J. Am. Chem. Soc.* **2022**, *144*, 12247.
[66] H.-H. Fang, S. Adjokatse, S. Shao, J. Even, M. A. Loi, *Nat. Commun.* **2018**, *9*, 243.
[67] S. A. Bretschneider, F. Laquai, M. Bonn, *J. Phys. Chem. C* **2017**, *121*, 11201.
[68] C. Li, J. Yang, F. Su, J. Tan, Y. Luo, S. Ye, *Nat. Commun.* **2020**, *11*, 5481.
[69] J. Fu, M. Li, A. Solanki, Q. Xu, Y. Lekina, S. Ramesh, Z. X. Shen, T. C. Sum, *Adv. Mater.* **2021**, *33*, 2006233.
[70] V. A. Hintermayr, L. Polavarapu, A. S. Urban, J. Feldmann, *ACS Nano* **2018**, *12*, 10151.
[71] Z. Fang, M.-H. Shang, Y. Zheng, Q. Sun, Y. Xu, X. Hou, W. Yang, *J. Phys. Chem. Lett.* **2023**, *14*, 6592.
[72] Y. Zheng, Z. Fang, M. Shang, Q. Sun, J. Zheng, Z. Yang, X. Hou, W. Yang, *ACS Energy Lett.* **2021**, *6*, 2328.
[73] A. H. Proppe, A. Johnston, S. Teale, A. Mahata, R. Quintero-Bermudez, E. H. Jung, L. Grater, T. Cui, T. Filleter, C.-Y. Kim, S. O. Kelley, F. De Angelis, E. H. Sargent, *Nat. Commun.* **2021**, *12*, 3472.
[74] A. Mahata, D. Meggiolaro, L. Gregori, F. De Angelis, *J. Phys. Chem. C* **2021**, *125*, 10901.
[75] Z. Fang, M.-H. Shang, Y. Zheng, Q. Sun, X. Hou, W. Yang, *J. Phys. Chem. Lett.* **2023**, *14*, 7331.